

Faster Switching at the VLA

C.L. Carilli, M.A. Holdaway, and K.P. Sowinski

National Radio Astronomy Observatory

Socorro, NM, 87801

May 13, 1996

Abstract

We analyze the fast switching phase calibration technique for correcting tropospheric phase variations at the VLA. We also perform observational tests of fast switching using a new ‘nodding’ mode at the VLA which allows for total cycle times as short as 40 seconds. Our analysis shows that there should be enough calibrators in the sky to capitalize on a 40 sec cycle time at all VLA frequencies. Also, analysis of the expected rms phase errors with a 40 second cycle time imply that it is unnecessary to alter the on-line system further in order to reduce the minimum cycle time to less than 40 seconds.

A series of test observations of fast switching phase calibration was performed at 22 GHz and 45 GHz. The results are consistent with theoretical predictions, and show that the fast switching technique is effective at ‘stopping’ tropospheric phase variations at an effective baseline of length $\approx \frac{v_a t}{2}$, where v_a = velocity of troposphere, and t = total cycle time. The residual rms phase noise is *independent of baseline length*. For a 40 sec cycle time the saturation value for the rms phase variations will typically be about 10° on winter nights, 15° on winter days or summer nights, and 30° on summer days, at 43 GHz.

We consider situations in which fast switching phase calibration will be required. We show that, even in good weather conditions, tropospheric ‘seeing’ will limit image resolution to at best 250 mas at 45 GHz (\approx C array resolution), if no tropospheric phase calibration technique is employed. Hence, the primary driver for implementing fast switching phase calibration at the VLA is to obtain images of faint sources with *diffraction limited spatial resolution on arbitrarily long baselines*.

1. Introduction

Fast switching involves standard phase calibration using a nearby calibrator source, only at a rate fast enough to ‘stop’ phase variations due to the troposphere. The technique was proposed, and demonstrated, by Holdaway and Owen (1995), Holdaway, Owen, and Rupen (1994), and Holdaway (1992). Holdaway’s analysis emphasized using the technique in the context of the MMA, for which tropospheric phase variations can lead to very short coherence times.

The addition of a 7mm system at the VLA raises the issue of implementing calibration techniques designed to reduce tropospheric phase variations, in particular for the larger arrays. Herein we reproduce Holdaway’s fast switching analysis in the context of the VLA at high frequency. We then present recent test observations using a new ‘nodding’ mode at the VLA. These tests demonstrate the power of the fast switching technique to minimize tropospheric phase variations on arbitrarily long baselines. We then outline situations in which the fast switching technique will be required to meet the scientific goals.

2. The Theory of Phase Variations due to the Troposphere

Phase variations due to the troposphere are caused predominantly by temporal changes in the water vapor content. The implied changes in index of refraction are non-dispersive, and hence the phase-variations will increase linearly with frequency. For completeness we note that tropospheric opacity at cm wavelengths is mainly due to the dry atmosphere (molecular oxygen), which does not vary substantially on diurnal timescales, while the liquid water content (clouds) contributes opacity (due to scattering), but does not alter phases substantially.

Tropospheric phase fluctuations can be characterized by a structure function, $D(b)$, where $D(b)$ is the square of the expected RMS phase variation, $\Phi_{rms}(b)$, on a baseline of length b , when averaged over a sufficiently long time $>>$ baseline crossing time = $\frac{b}{windspeed}$, or for an ensemble of measurements at a given time on many baselines of length b . Heretofore we designate $\Phi_{rms}(b)$ as the ‘root structure function’. Kolmogorov turbulence theory (Coulman 1990) predicts a function of the form:

$$\Phi_{rms}(b) = \frac{K}{\lambda} b^n \quad degrees \quad (1)$$

where b is in km, λ is in cm, and K is given below. The power-law index n has different values depending on the nature of the turbulent layer on a given day, and on the baseline length (Holdaway et al 1995). Adopting a simple model of a turbulent boundary layer at a height of 1 km with a width of 1 km, the prediction is: $n = \frac{1}{3}$ for baselines longer than 1 km, and $n = \frac{5}{6}$ for baselines shorter than 1 km. The change in power-law index at 1 km baseline length is due to the finite width of the turbulent boundary layer. For baselines shorter than the typical boundary layer width the full 3-dimensionality of the turbulence is involved, while for longer baselines a 2-dimensional (thin-screen) approximation applies. This basic broken power-law root structure function has been observed with the VLA in a number of instances (Sramek 1990), although power-laws of intermediate indices have also been seen (Holdaway and Owen 1995, Holdaway et al. 1995).

The constant K corresponds to the normalization value at 1 km, and it varies with the weather. In this memo we will adopt the broken power-law function of Sramek (1990), in which he found for typical conditions on winter nights at the VLA $K = 22$, while for summer nights and winter days $K = 33$, and for summer days $K = 58$. A sample $\Phi_{rms}(b)$ curve for the VLA is plotted in Figure 1 for a few select frequencies.

An important point to keep in mind is that while tropospheric phase variations can be quantified in terms of a baseline-length dependent structure function, the errors are fundamentally antenna-based, and hence can be corrected by antenna-base calibration schemes, such as self-calibration or fast switching calibration. This dual-nature of tropospheric phase variations relates simply to the fact that the excess electrical pathlength due to the tropospheric water vapor content for two antennas is correlated over some timescale set by the baseline length, the wind speed, and the phase structure function. For instance, the excess phase due to large-scale structure in the troposphere will be correlated between two closely spaced antennas, ie. short baselines only ‘sample’ the power in the phase structure function on scales \leq the baseline length.

A final point is that there may be an ‘outer-scale’ beyond which the rms phase fluctuations saturate. This outer-scale is set simply by the outer-scale in the tropospheric turbulence, and is hypothesized to be

around 10 km (Coulman 1990). The existence of such an outer scale remains to be verified observationally (Sramek 1990).

3. Fast Switching

Fast switching entails switching between the target source and a bright calibrator on timescales shorter than the baseline crossing time for the troposphere. Holdaway (1992) shows that the expected residual phase fluctuations after fast switching calibration is applied are:

$$\Phi_{rms} = [D(\frac{v_a t}{2} + d)]^{\frac{1}{2}} \quad (2)$$

where v_a = wind speed, t = total cycle time, and d = the physical distance in the troposphere between the calibrator and source. The baseline-dependent term, $D(b)$, is calibrated-out, and one is left with residual phase variations as expected for a baseline of effective length:

$$b_{eff} = d + \frac{v_a t}{2} \quad (3)$$

Obviously the technique will only be effective for timescales much shorter than $\frac{b}{v_a}$. Moreover, a significant gain is made when $b_{eff} < 1$ km, thereby allowing for corrections to be made on the steep part of the phase structure function (see Figure 1).

The technique of tropospheric phase calibration by fast switching was successfully demonstrated in a test observation with the VLA at 22 GHz (Holdaway and Owen 1995). However, the cycle time was limited by the 20 seconds lost in start-up overhead at the beginning of each VLA scan. Hence, the minimum cycle time was about 80 seconds for the VLA in its standard mode. A new observing mode has been implemented for the VLA, involving ‘nodding’ observations using offset cards. In this mode there is no 20sec start-up time, and the cycle time is set simply by the antenna slew rate, the source-calibrator distance, and the desired time on target source and calibrator. This mode allows for cycle times as short as 40 seconds. This mode is under development, and is currently not available for general use (as of May 1996).

The first question to address when considering implementing fast switching as a standard observing mode at the VLA is: are there enough calibrators in the sky in order to take advantage of a switching

time as short as 40 seconds? As shown by Holdaway (1992), this question can be addressed by minimizing the quantity: $[d + \frac{v_a t}{2}]$ as a function of calibrator strength, given an estimate of the sky density of calibrators as a function of frequency and flux density, and given various system parameters (sensitivity, slew rate...). Holdaway performed this analysis for the MMA. We repeat the analysis for the VLA at various frequencies. The basic equation is:

$$d + \frac{v_a t}{2} = \frac{h}{\sin(\text{el})} \sin[7.1(\frac{\nu}{90})^\alpha S_\nu^{0.75}] + X \frac{v_a}{2} [C_\nu^2 R^2 S_\nu^{-2} + \frac{14.2}{v_s} (\frac{\nu}{90})^\alpha S_\nu^{0.75}] \quad \text{meters (4)}$$

where:

h = typical height of tropospheric turbulence in meters. We use $h = 1000\text{m}$.

ν = observed frequency in GHz.

α = power-law index for the source population density, $\phi_{S,\nu}$, as given by:

$$\phi_{S,\nu} = 7.1(\frac{\nu}{90})^{-\alpha} S_\nu \quad \text{degrees}$$

where $\phi_{S,\nu}$ is the average distance between calibrators with flux density S_ν (Jy) at frequency ν (GHz) (Holdaway, Owen, and Rupen 1994). We assume $\alpha = 0.5$.

el = source elevation. We do all calculations at $\text{el} = 60^\circ$

$X = \frac{t_{cyc}}{t_{cyc} + t_{src}}$, where t_{cyc} = total cycle time, and t_{src} = time on target source. We use $X = 3$, which implies 1/3 of total cycle time is spent on the target source.

C_ν = a constant relating to the system sensitivity per baseline. For the VLA the parameter for the different bands is: $C_\nu = 0.053, 0.16, 0.26, 0.43$, for X, U, K, and Q bands, respectively.

R = required signal-to-noise per baseline. The expected phase errors for antenna-based calibration are then: $\frac{0.7 \text{ rad}}{R(N_{ant}-3)^{0.5}}$, where N_{ant} is the number of antennas. We use $R = 2$.

v_s = slew rate. The slew rate of the VLA is $0.66^\circ/\text{sec}$ in elevation and $0.33^\circ/\text{sec}$ in azimuth, although in practice these slew rates are only reached for moves larger than 2° . We adopted a value of $0.5^\circ/\text{sec}$.

S_ν = the calibrator flux density in Jy.

v_a = tropospheric velocity. We use $v_a = 15 \text{ m/sec}$.

The first term in equation 4 is the ‘d’ term. The second term is dictated by the array sensitivity, and the third term relates to the slew distance. Note that there is no set-up time term for the VLA when using the nodding mode, hence the lack of a forth (constant) term in equation 4 as was required for the MMA analysis.

Curves for $[d + \frac{v_{st}}{2}]$ at different VLA frequencies are shown in Figure 2. Values for minimum cycle times, optimum calibrator flux densities, and implied slew distances are given in Table 1. In practice for the VLA at high frequency the ‘d’ term is typically an order of magnitude less than the $\frac{v_{st}}{2}$ term. The conclusion from Figure 2, or Table 1, is clear: **There should be enough calibrators in the sky to capitalize on a 40 sec cycle time at all VLA frequencies.** Of course, this is a statistical statement, and does not reflect the incompleteness in the current VLA calibrator lists.

A 40 sec cycle time implies an effective baseline of length $\approx 300\text{m} \approx \frac{v_{st}}{2}$. For longer spacings the tropospheric phase fluctuations are essentially stopped by fast switching. From Figure 1 one can see that the implied ‘saturation value’ for the rms phases even under moderate conditions (winter days, summer nights) is no worse than 15° at the highest VLA frequency. The expected image dynamic range under such conditions, and using 13 antennas, is 50. Hence, a second important conclusion is: **Analysis of expected rms phase errors with a 40 second cycle time imply that it is unnecessary to alter the on-line system further in order to reduce the minimum cycle time to less than 40 seconds.**

A final point to keep in mind is that self-calibration can be performed with a 40 second averaging time on sources stronger than about 100 mJy at 43 GHz. Fast switching is not required in these cases.

4. Tests of Fast Switching at the VLA

A test of fast switching was performed at the VLA the night of March 4, 1996. The VLA was in C configuration and tests were performed at both 22 GHz and 43 GHz. The sources observed were four VLA calibrators all situated within 4° of each other. All the sources are stronger than 2 Jy at the observed frequencies. The source 3C345 (1641+399) was chosen as the ‘calibrator’, and nodding observations were made of the three ‘target’ sources, situated at distances of 0.4° (1638+398), 2.2° (1633+382), and 3.7°

(1624+416) from 3C345. A total of about 20 minutes was spent observing each calibrator-target source pair, at each frequency. Offset pointing corrections were measured at 8 GHz on 3C345, and applied at all frequencies.

The observations employed a total cycle time of 40 sec, split evenly between the calibrator and the target source, including slew time. We used an integration time of 1.6 sec. The resulting number of valid records on-source for the three target sources above were: 8, 6, and 3, respectively, out of a maximum of 12 records in 20 secs.

The nodding data are stored as a series of 20sec scans in the exact same way as would be expected if source cards were employed. The source names default to the source positions. Hence, the data can be calibrated within AIPS in exactly the same way as for the normal VLA set-up. Antenna-based amplitude and phase solutions were generated for each 20 second scan on the calibrator. These solutions were then averaged over different time-scales, and applied to the target sources, to test the behavior of fast switching vs. switching time. (Note: short time-averaging applies only to the phase solutions. Amplitude solutions were averaged over a long time scale in all cases).

In order to calculate the root phase structure function, the single source calibrated data were written to a disk-FITS file, and further processing was performed using the SDE software package. The program PHRMS in SDE calculates the root phase structure function by computing the rms phase variation on a given baseline over the observation period. (Note: a negligible error is introduced by the fact that the baseline length may change over the observation period). These values can then be binned in baseline-length to improve SNR.

The results for the root phase structure function without any baseline-binning are shown in Figure 3 for 22 GHz data on the closest of the target sources. Figure 3A shows the results for an averaging time of 1200 secs $\approx 4 \times$ the array crossing time for the troposphere. Figure 3B shows the results for the fast switching averaging time of 40 seconds. The long-averaging time data reveals the nominal root phase structure function for the troposphere that night. One can see that even without fast switching, the phase stability was very good during these observations, with a maximum RMS value of about 20°

on a 3 km baseline. This structure function is also shallower than is normal for the VLA, with a slope of 0.45 for baselines shorter than 1km, and 0.25 for baselines longer than 1 km.

Still, the effectiveness of the fast switching technique can be seen in Figure 3B, where the rms phase variations ‘saturate’ at a value of about 8° at around 300m baseline, and remain constant to the longest baselines. This effect is better demonstrated in Figure 4, which shows the rms phase variations after binning in baseline length. The top panel is for a 1200 sec averaging time, the middle panel is for a 120 sec averaging time, and the bottom panel is for a 40 sec averaging time. Again, the 1200 sec cycle time shows the nominal structure function for that night. When using shorter averaging times the rms phase follows the nominal root structure function for baselines shorter than: $d + \frac{v_a t}{2}$, beyond which the rms values are no longer baseline-dependent. Overall, we conclude that: **The fast switching technique is effective at ‘stopping’ tropospheric phase variations at an effective baseline of length $\approx \frac{v_a t}{2}$, and the residual rms phase noise beyond b_{eff} is independent of baseline length.**

Indeed, one can calculate the velocity of the troposphere from the baseline length at which the rms phase variations saturate for a given cycle time. We obtain: $v_a = 16 \pm 4$ m/sec. These tests verify the results of Holdaway and Owen (1995), thereby demonstrating the effectiveness of tropospheric phase calibration via fast switching at the VLA.

The results for the 2.2° distance target source are shown in Figure 5. These results are essentially the same as for the closer calibrator. We do not display results for the 3.7° source, due to the paucity of data for this source. The results at 43 GHz are displayed in Figure 6. Again, the technique is effective, although the lack of baselines longer than 1 km at 43 GHz in this array does not allow us to sample the ‘break’ in the structure function.

The final point to consider is the effect of the fast switching technique in the image-plane. Unfortunately, the phase stability for these test observations was very good, hence the improvement in the image-plane will not be as dramatic as it may be under worse conditions. Still, the effect can be seen on the images in Figure 7. Figure 7A shows a uniformly weighted image made from data with a calibration cycle time of 5 minutes – typical for most high frequency observations at the VLA. Figure 7B shows an

image made from data with 40 sec averaging. The image fidelity, as measured by the ratio of the peak surface brightness relative to peak sidelobe, goes from 83 for the 300 sec image, to 99 for the 40 sec image. A similar improvement is seen for natural weighting.

5. When is Fast Switching Required?

There are two areas in which tropospheric phase calibration through fast switching may be important. The first is the dynamic range limitation set by phase errors. The nominal limit is: $DNR \approx \frac{N_{ant}}{\Phi_{rms}}$, where N_{ant} = number of antennas, and Φ_{rms} = rms phase in radians. For example, under moderate conditions at 43 GHZ for the VLA, equation (1) leads to: $DNR = \frac{80}{t_{cyc}^{0.33}}$, for baselines longer than 1 km. Even for fairly long averaging times the expected DNR limit is not severe, $DNR \approx 12$ with $t_{cyc} = 300$ seconds. Hence, for simple detection experiments in most arrays under moderate to good weather conditions, the loss in SNR due to time spent switching between source and calibrator out-weighs the gain in DNR due to lower phase errors.

The driver behind implementation of fast switching at the VLA is: **To obtain images of faint sources with diffraction limited resolution on arbitrarily long baselines.** Narayan et al. (1990) discuss the impact of atmospheric phase variations on image quality and resolution. An order-of-magnitude estimate of the size of the ‘seeing-disk’ is set by:

$$\Theta_s = \frac{\lambda}{r_o}, \quad (5)$$

where λ = observing wavelength, and r_o = the transverse scale over which the rms phase difference is of order a radian. This size corresponds roughly to the expected FWHM of the image size due to tropospheric phase fluctuations for an image made from data covering a time period much longer than the array crossing time of the troposphere (ie. data sampling many realizations of the phase screen). Of course, the detailed shape of the seeing disk depends on the phase structure function. Using equation (1) leads to:

$$\Theta_s = 1 \times 10^{-5} \frac{K^3}{\lambda^2} \text{ arcsec} \quad (6)$$

In Table 2 the value of r_o is listed for the different weather conditions at the VLA, with the corresponding

values of θ_s . The implication is clear: even under the best weather conditions, the expected resolution of the VLA will be limited to 250 mas (\approx C array resolution) by tropospheric 'seeing' at 43 GHz. To avoid this limit, either self-calibration must be employed on short times scales, or some technique, such as fast switching, must be employed to calibrate-out the tropospheric phase variations. Again, the practical lower limit for self-calibration using a 40 sec averaging time is about 100 mJy at 43 GHz at the VLA. For weaker sources, fast switching is the only alternative currently available.

6. Other Limitations at the VLA

There are two other factors in the current VLA on-line system which limit the use of the nodding mode of observation. The first is the maximum data rate. Using a 1.6 second averaging time and 13 antennas allows for a maximum of 128 channels with one polarization. The second is that the observing mode cannot be changed between the target source and calibrator. Hence, if the target source is being observed with a narrow bandwidth in spectral line mode, the calibrator must use the same bandwidth and same line mode. The decreased sensitivity with a narrow bandwidth may require longer integration times on the calibrator.

References

- Coulman, C.E. 1990, in *Radio Astronomical Seeing*, eds. J. Baldwin and S. Wang, (Pergamon: New York), p. 11.
- Holdaway, M.A., Radford, S., Owen, F., and Foster, S. 1995, MMA Memo. Series.
- Holdaway, M.A. and Owen, F.N. 1995, MMA Memo. No. 126
- Holdaway, M.A. Owen, F., and Rupen, M.P. 1994, MMA Memo. No. 123
- Holdaway, M.A. 1992, MMA Memo. No. 84
- Narayan, R., Anatharamiah, K., and Cornwell, T. 1990, in *Radio Astronomical Seeing*, eds. J. Baldwin and S. Wang, (Pergamon: New York), p. 205.
- Sramek, R. 1990, in *Radio Astronomical Seeing*, eds. J. Baldwin and S. Wang, (Pergamon: New York), p. 21

Table 1: Optimum Fast Switching Parameters

Frequency GHz	Calibrator Flux Density Jy	$d + \frac{v_s t}{2}$ meters	t_{cyc} seconds	Θ_{slew} degrees
43	0.38	212	22	2.4
22	0.30	126	13	1.4
15	0.22	84	8.8	0.9
8	0.11	37	3.8	0.4

Table 2: Tropospheric Seeing Parameters at 43 GHz

	Summer Days	Winter Days	Winter Nights
Θ_s	4.5"	0.8"	0.25"
r_o	320m	1900m	5800m

FIGURE CAPTIONS

Figure 1: The root phase structure function, $\Phi(b)$, for the VLA at various frequencies in weather conditions corresponding to typical winter days or summer nights (Sramek 1990).

Figure 2: Plots of the quantity $[d + \frac{v_{st}}{2}]$ versus calibrator flux density for various frequencies at the VLA.

Figure 3: The observed root phase structure function, $\Phi(b)$, for the VLA at 22 GHz in C array from observations the night of March 4, 1996. Figure 3A shows the data using a calibration cycle time of 1200 sec $\approx 4 \times$ nominal array crossing time for the troposphere. Figure 3B shows the data using a 40 sec cycle time. The calibrator-source distance was 0.4° , and no baseline-binning was employed.

Figure 4: The observed root phase structure function, $\Phi(b)$, for the VLA at 22 GHz in C array from observations the night of March 4, 1996. In this case, baseline-binning was employed, with a bin-width of 30m. Figure 4A shows the data using a calibration cycle time of 1200 sec. Figure 4B shows the data using a 120 sec cycle time, and Figure 4C shows the data with a 40 sec cycle time. The calibrator-source distance was 0.4° .

Figure 5: Same as Figures 4A and 4C, but for a source-calibrator distance of 2.2° .

Figure 6: Same as Figures 4A and 4C, but at 43 GHz.

Figure 7: Images of 1638+398. Figure 7A was made from data using a calibration cycle time of 300 sec. Figure 7B was made from data using a calibration cycle time of 40 sec.

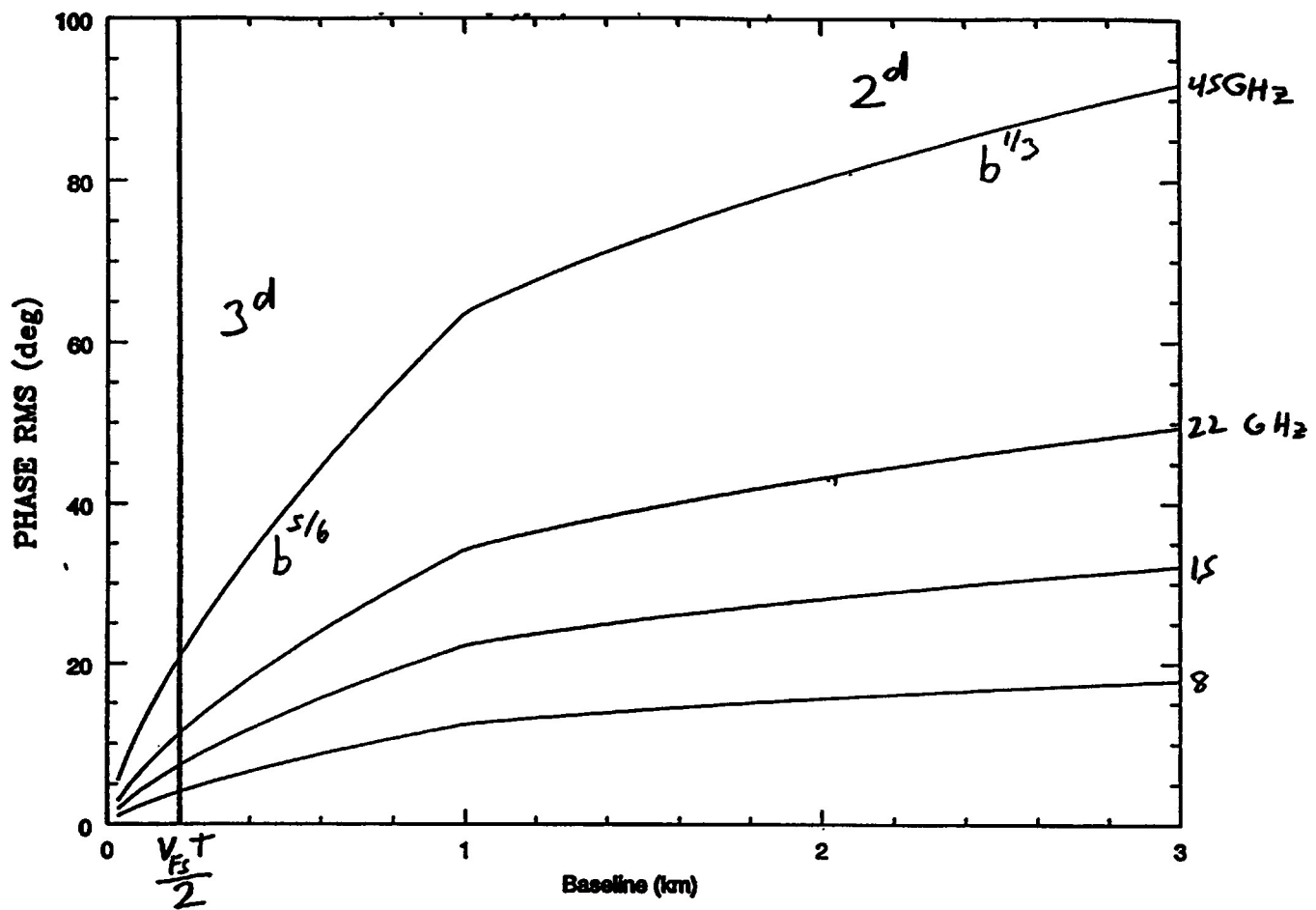


Figure 1

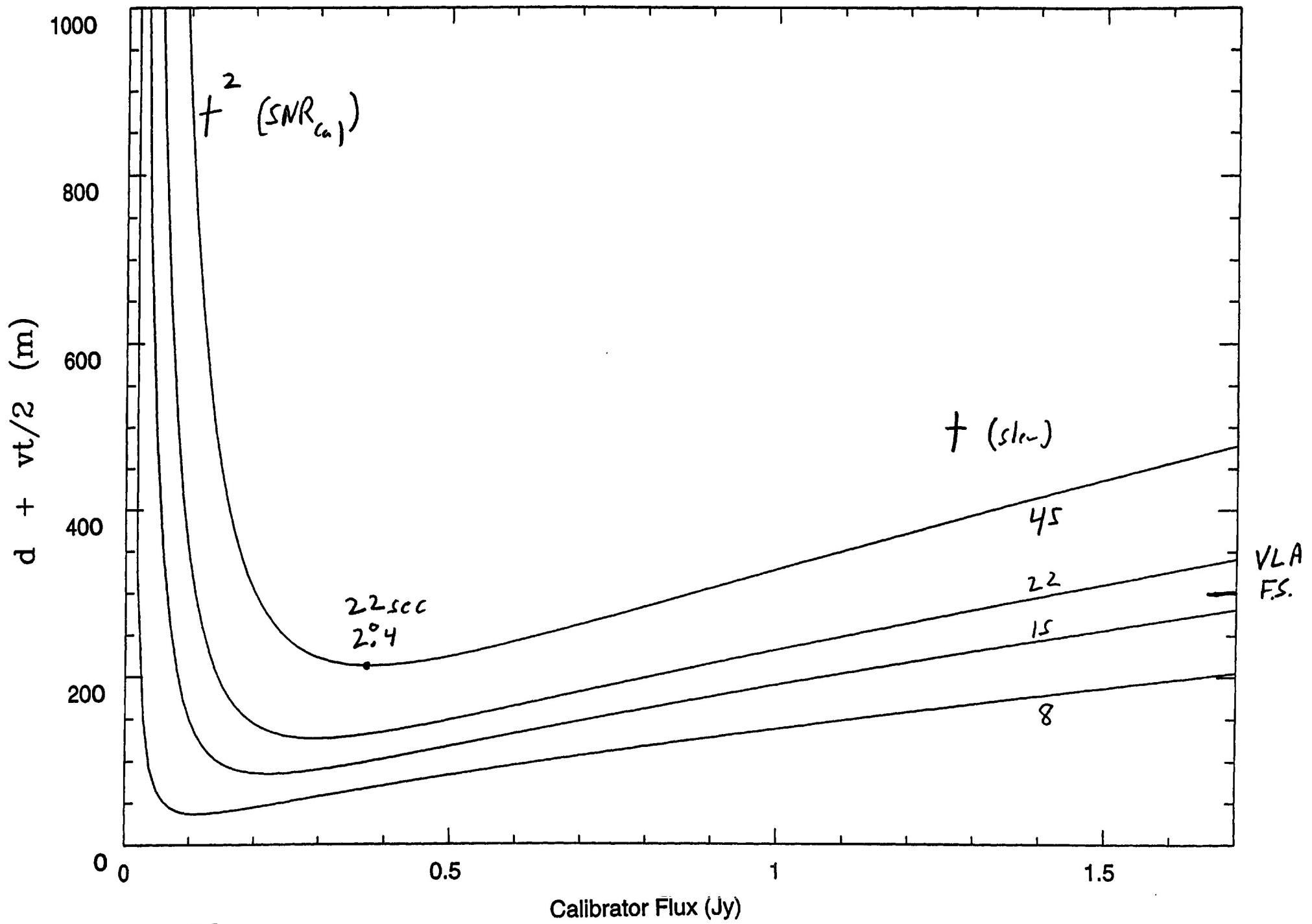


Fig. 2

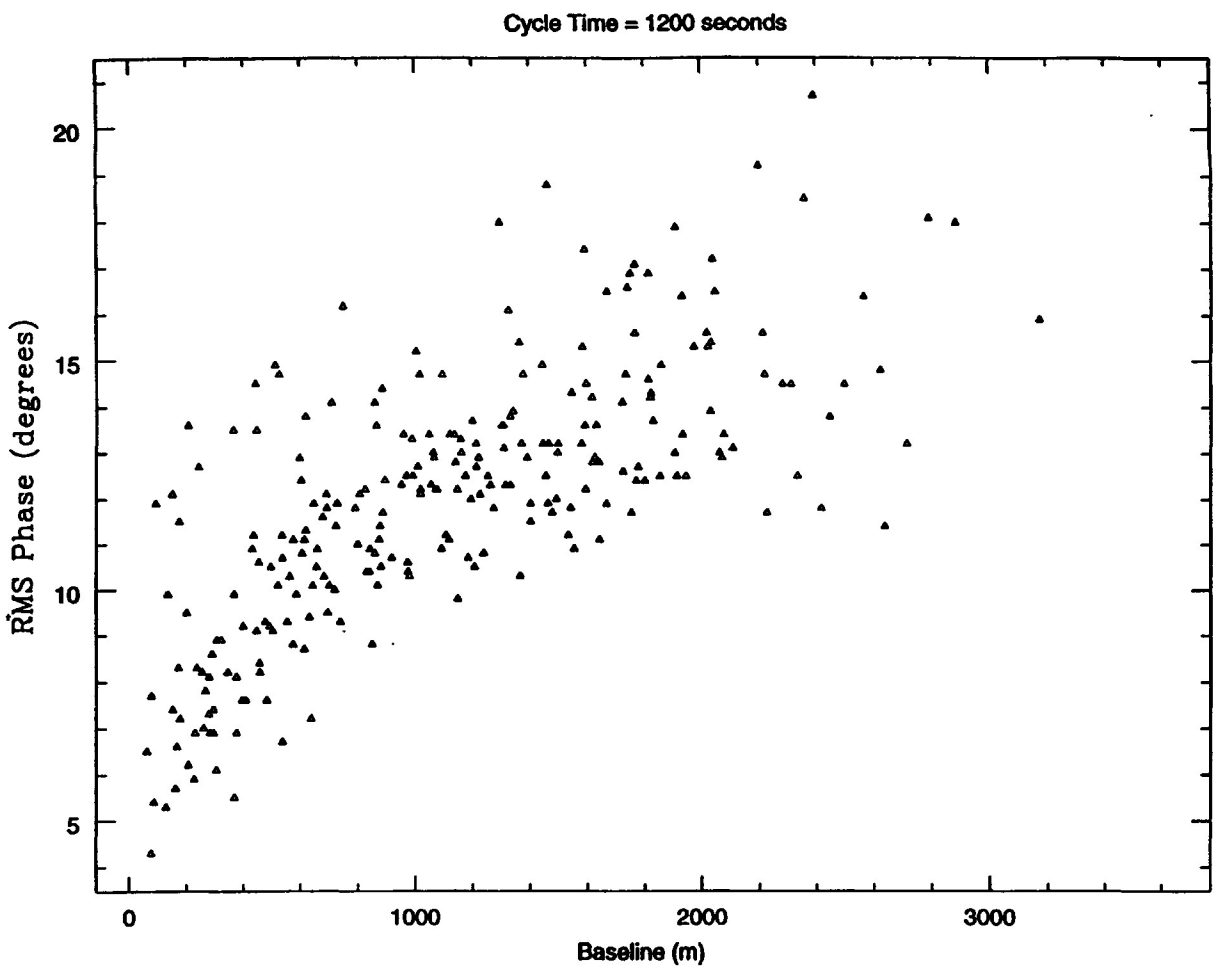


Fig.
3

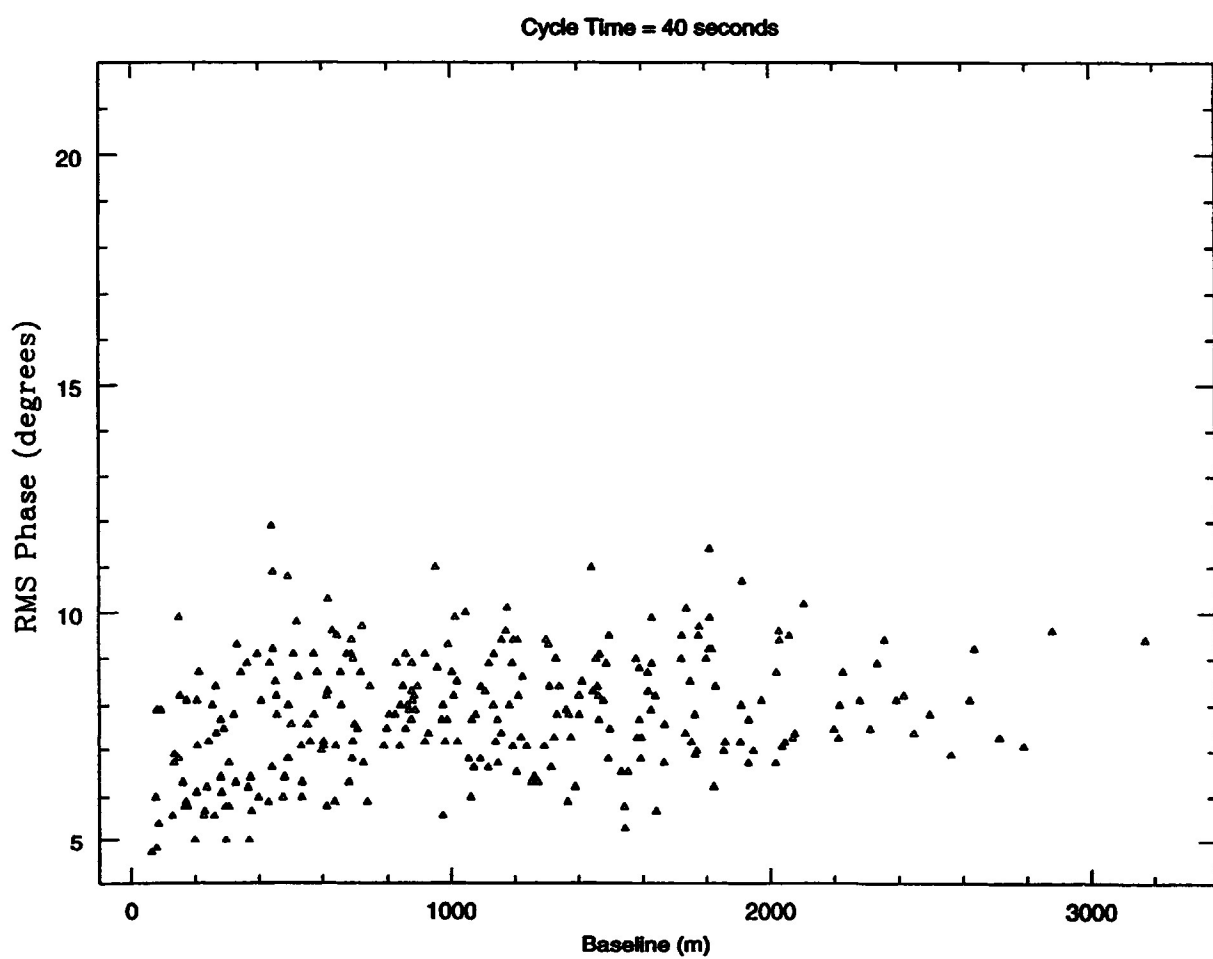
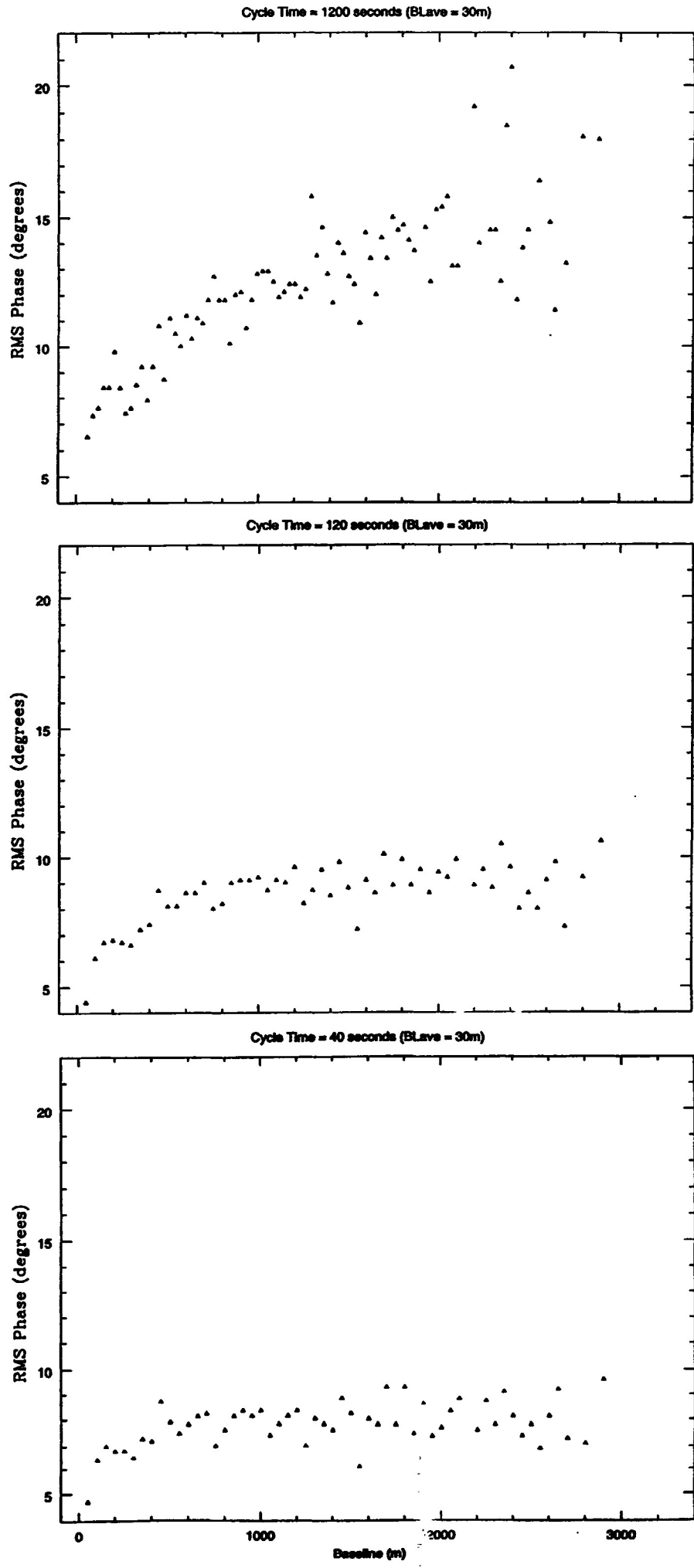
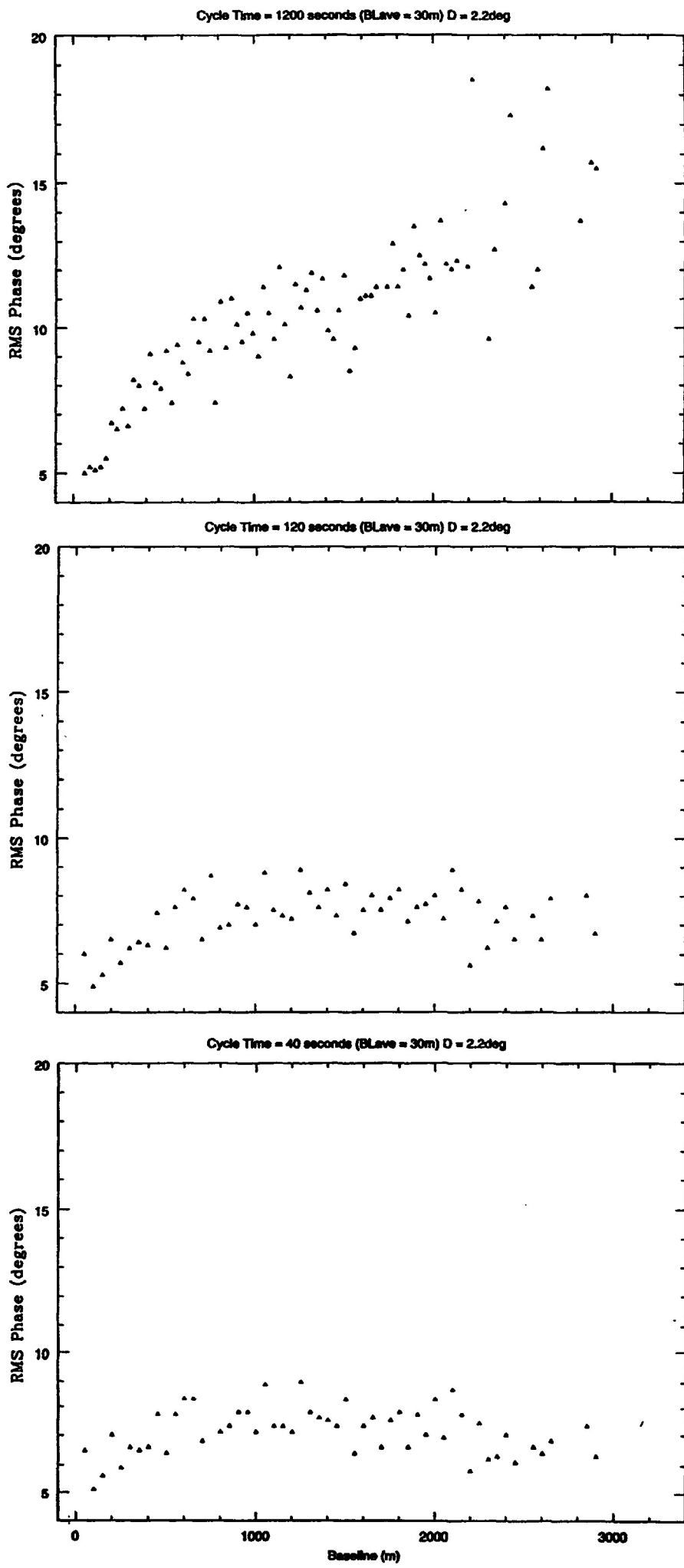


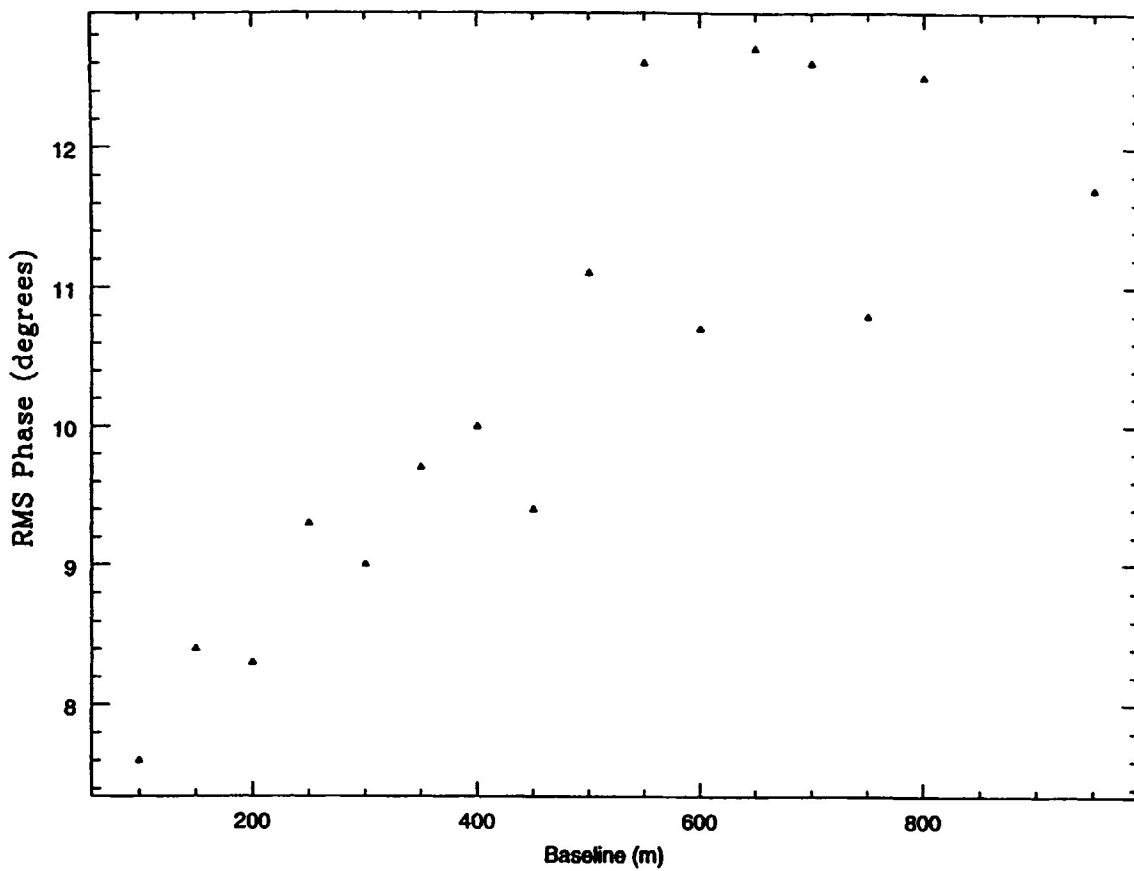
Fig 4





5 Fig

Cycle Time = 600 seconds; Ave BL = 50m; D = 0.4deg; 43 GHz



Cycle Time = 40 seconds; Ave BL = 50m; D = 0.4deg; 43 GHz

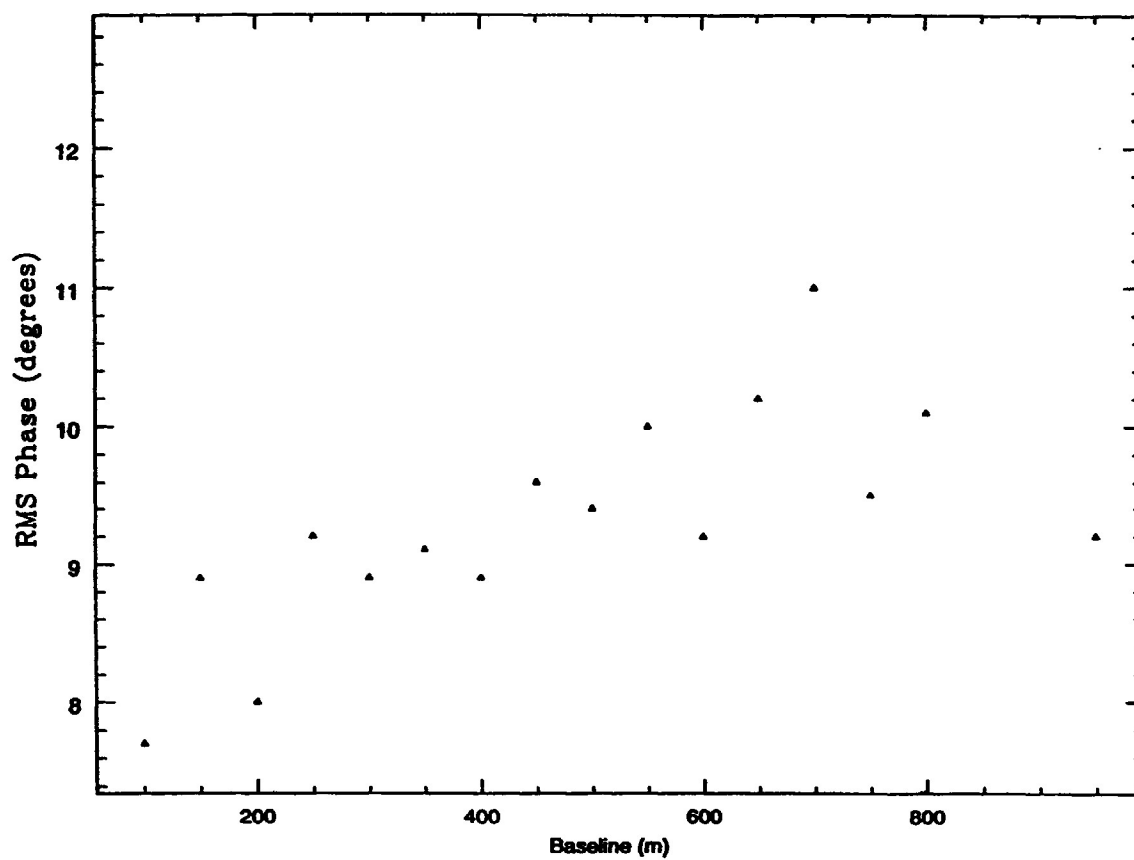
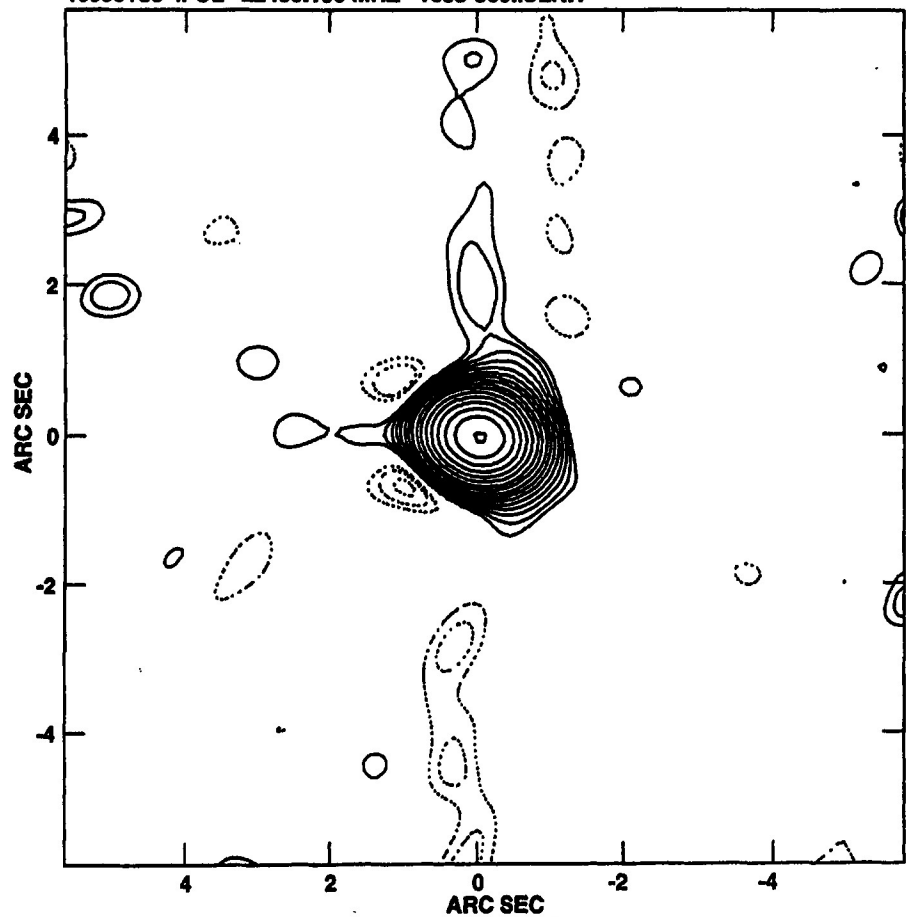


Fig. 6

PLot file version 4 created 15-APR-1996 10:17:43
16388+39 IPOL 22485.100 MHZ 1638-300.ICLN.1

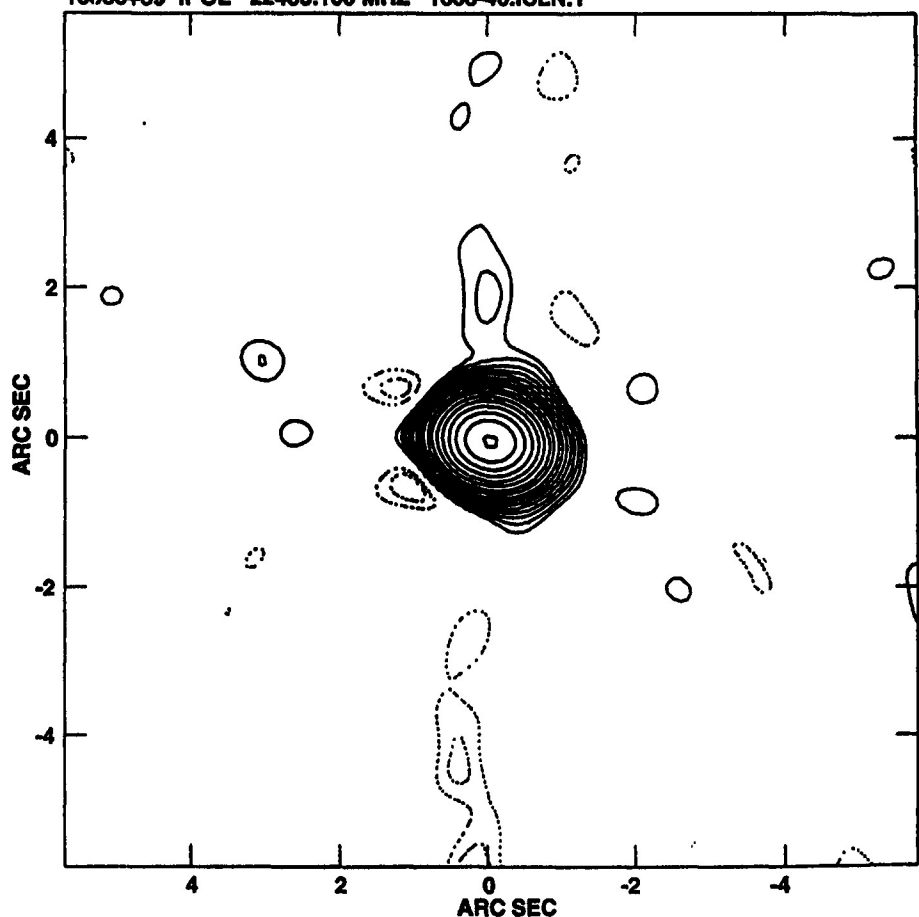


Center at RA 16 38 48.17274 DEC 39 52 30.1140

Peak flux = 1.6697E+00 JY/BEAM

Levs = 9.0000E-03 * (-4.00, -2.80, -2.00,
-1.40, -1.00, 1.00, 1.400, 2.000, 2.800,
4.000, 5.700, 8.000, 11.00, 16.00, 22.00,
32.00, 45.00, 64.00, 91.00, 128.0, 182.0,
256.0)

PLot file version 3 created 15-APR-1996 10:17:58
16388+39 IPOL 22485.100 MHZ 1638-40.ICLN.1



Center at RA 16 38 48.17274 DEC 39 52 30.1140

Peak flux = 1.6650E+00 JY/BEAM

Levs = 9.0000E-03 * (-4.00, -2.80, -2.00,
-1.40, -1.00, 1.00, 1.400, 2.000, 2.800,
4.000, 5.700, 8.000, 11.00, 16.00, 22.00,
32.00, 45.00, 64.00, 91.00, 128.0, 182.0,
256.0)

Fig 7